Journal of Materials Chemistry B

ROYAL SOCIETY OF CHEMISTRY

PAPER

View Article Online
View Journal | View Issue



Cite this: J. Mater. Chem. B, 2022, 10, 2740

# Dual-responsive zwitterion-modified nanopores: a mesoscopic simulation study†

Zhaohong Miao, Zheng Chen, Li Wang, Lizhi Zhang and Jian Zhou *

Received 5th November 2021,
Accepted 8th March 2022

DOI: 10.1039/d1tb02416g

rsc.li/materials-b

In this work, dissipative particle dynamics simulation was carried out to investigate the intelligent switching effect of nanopores grafted by the zwitterionic polymer brushes poly(carboxybetaine) with excellent antifouling properties. The result shows that with different grafting densities and grafting lengths, zwitterionic polymer brushes show typical pH- and salt-responsiveness features. When the grafting density is greater than 0.2 accompanying a grafting length of 40, pH has a significant effect on the structure and pore size of the nanopores, that is, the pore remains open under neutral condition and exhibits a switching effect under acidic condition. Similarly, the size of the nanopore can be tuned by altering the grafting density and polymer chain length under salt-concentration-responsive conditions. Differently, compared with the pH effect, the salt concentration has an obvious impact on the switching effect, *i.e.*, responsiveness emerges with a lower grafting density and length. This work provides molecular level mechanism and theoretical guidance for the design of smart nanopores modified by zwitterionic polymer brushes, as well as plays an important role in the construction of nanopores with antifouling and pH/salt-responsive properties.



## Introduction

Anti-fouling is one of the most crucial requirements in biomaterials-related engineering fields.[1–7] Three generations of anti-fouling polymer materials have been successively dug out and studied: 2-hydroxyethyl methacrylate (HEMA)-based polymers,[8,9] PEGylated-based polymers[10–12] and zwitterionic-based polymers.[13,14] Although the first two generations of materials display good anti-fouling performance based on their hydrophilicity, their property is still limited under complex conditions, which leads to the reduction of their anti-fouling ability.[15–18] Inspired by the cell membrane structure, zwitterionic-based polymers based on the natural bio-inert theory have been developed, which have equal positive and negative charges.[13,14,19,20] Therefore, zwitterionic polymers exhibit their antifouling properties due to the strong electrostatic interactions with surrounding water molecules which facilitates the formation of a stronger hydration layer compared with the hydration layer formed by the H-bond interaction in (HEMA)-based and PEGylation-based polymers. Because of the bionic characteristics and outstanding anti-fouling properties, zwitterionic-based materials have been explored more and more deeply in the past decade, and have been proved as a preferred candidate for surface modification in biomedical and engineering applications as well as in membrane science of flow control, such as biomedical membranes, desalination membranes, and chemical sensor membranes.[21–26] In more detail, Vinod *et al.* summarized a series of bio-inspired strategies for designing antifouling biomaterials. In their review, a list for comparison of various antifouling strategies had been presented; zwitterionic polymers, as a typical chemical modification material, possess prominent advantages, such as long-term antifouling characteristics and unique capability for ligand immobilization.[27] As Banerjee *et al.* summarized in their review, to fabricate antifouling coating, zwitterionization is one of the best options for resisting proteins.[1] Additionally, Fam *et al.* explored the efficient stealth coating of nanoparticles in drug delivery systems, in which the polyzwitterions with superior ionic solvation, created highly hydrophilic surfaces to reduce protein adsorption, and resolved the limitation of stability.[28] Moreover, Sin *et al.* overviewed studies focused on hemocompatibility of zwitterionic interfaces and membranes. They illustrated the development of antifouling materials in detail, especially zwitterionic polymers; they further introduced the fabrication and applications of zwitterionic interfaces and membranes, which proved that zwitterionic polymers are promising materials in the biomedical field.[29]

Additionally, porous membranes, with intelligent responsiveness that can respond to environmental factors such as pH, temperature, ionic strength, electric fields, *etc.*, have been paid

*School of Chemistry and Chemical Engineering, Guangdong Provincial Key Lab for Green Chemical Product Technology, South China University of Technology, Guangzhou, Guangdong, 510640, P. R. China. E-mail: jianzhou@scut.edu.cn; Fax: +86 20 87114069; Tel: +86 20 87114069*

† Electronic supplementary information (ESI) available. See DOI: 10.1039/d1tb02416g

special attention in recent years.[30–34] Chu and coworkers summarized the stimuli-responsive membranes and proved the important role of smart membranes in separation processes.[35] Moreover, Liu *et al.* summarized the developments in various stimuli-responsive smart gating membranes, in which the zwitterionic material, as a typical polyelectrolyte material, plays a key role in the ion-strength-responsive gating.[36] Palivan *et al.* introduced bioinspired polymer vesicles and membranes for biological and medical applications. In their work, it was shown that the intrinsic stimuli-responsiveness is the most important property of biological membranes which is also the subject of artificial membranes.[37] In greater detail, the surface or pore characteristics and permeation properties (hydraulic permeability and diffusional permeability) of the stimuli-responsive membranes can be dramatically adjusted by the modification of functional materials which further realizes the flow control with an intelligent switching effect, especially in the field of micro/nano flow control.[38–41] Consequently, it has become increasingly important for the intelligent stimuli-responsive modification of nanopores. As for the definition of a nanopore, as mentioned in the article, it is considered that both ''nanopores'' and ''nanochannels'' are in common mutual use. In terms of shape, a nanopore is defined simply as a pore having a diameter in the range of 1 to 100 nm, with the pore diameter larger than its depth.[42] Nowadays, with the demand for the application of micro/nano flow control, based on the structure of the nanopore/nanochannel and the requirement of different properties, mass modifications of nanopore/nanochannel are being explored. For instance, Siwy *et al.* prepared a polyimide foil with a single asymmetric electro-responsiveness pore, namely, the effect of ion-current rectification can be strongly influenced by the surface charge of the pore, which can be regulated by the pH of the electrolyte.[43] Alem *et al.* modified the nanopore walls of the PET membrane by *N*-isopropylacrylamide (NIPAM) brushes. They found that the temperature modulated permeability properties of this responsive polymeric system showed a pore-size dependent character. That is, for larger pores ($\Phi \sim 330$ nm), as the PNIPAM chain conformations expanded (T < LCST), the pore size as well as the permeabilities decreased compared to the collapsed conformation, while for narrower pores ($\Phi \sim 80$ nm), the expanded PNIPAM brushes (T < LCST) offered greater hydration ability, resulting in improved permeability compared to that of the collapsed conformation.[44] Guo *et al.* fabricated a dual-functional nanofluidic device that integrated the ionic gate and the ionic rectifier within one solid-state nanopore which was realized by grafting temperature- and pH-responsive poly(-*N*-isopropyl acrylamide-*co*-acrylic acid) brushes onto the wall of a cone-shaped nanopore.[31] Wang *et al.* constructed a poly(ethylene terephthalate) film modified by immobilizing zirconium(IV) ions with a single nanopore, which showed biomimetic ion-responsiveness and could be used as an ionic sensor.[38]

Although stimuli-responsive membranes have been studied broadly, membrane fouling still restricts their application. Combining the advantages of zwitterionic materials, porous membranes have been further explored, and some interesting results have been obtained.[45] Nanopores in membranes modified with zwitterionic polymer brushes not only retain or even obtain more sensitive switching effects, but also display excellent anti-fouling performance, which is of great significance for the application.[42] For example, Yameen *et al.* synthesized single conical nanopores displaying pH-tunable rectifying characteristics, in which the zwitterionic polymer brushes modified in the surface of nanopores played an important effect in manipulating ionic transport.[46] Wang *et al.* fabricated a salt-responsive membrane with an ultrahigh gating ratio by grafting zwitterionic nanohydrogels onto a poly(acrylic acid)-grafting-poly(vinylidene fluoride) (PAA-*g*-PVDF) microporous membrane which realized highly sensitive responsiveness and anti-fouling simultaneously.[30]

Notwithstanding the progress achieved in the experimental study of stimuli-responsive nanopores modified by zwitterionic polymers, the molecular details of the structure and functions remain poorly understood, which further restricts their application in various fields, especially in microfluidic applications. Computer simulations can supplement the experimental work and facilitate the exploration of new achievements.[47,48] Nevertheless, some computer simulation studies have been carried out to explore the nanopore properties, and the structure–activity relationship is not well understood[49–51] for zwitterion-modified nanopores. Owing to the fact that physical phenomena observed at the macroscopic scale are essentially determined by the microstructure of matter, mesoscopic simulation actually serves as a bridge between molecular information and macroscopic properties. Dissipative particle dynamics (DPD) simulation which matches the temporal and spatial scale of polymer self-assembly behaviours has been proved to be one of the most effective methods to investigate polymer properties at the mesoscopic scale.[52–55] In this study, DPD simulation was performed to study the switching effect of nanopores modified by zwitterionic polymer poly(carboxybetaine) (PCBMA)[56,57] brushes, which is one of the most widely used technique and combines ultralow fouling and ease functionalization. The effects of chain length and grafting density of polymers on the smart switching of nanopores were studied under both neutral and highly acidic pH conditions, as well as different salt concentration conditions. The effects of pH and salt concentration on the nanopore switching and nanopore sizes were further compared. This study aims to explore the molecular mechanism of the switching effect of zwitterionic-polymer-modified nanopores and provides theoretical guidance for designing smart nanopores.

## Experimental

### Simulation method

**DPD method.** DPD, as a mesoscale simulation for complex fluid systems, was first introduced by Hoogerbrugge and Koelman[58] and later modified by Groot and Warren.[54] In the coarse-grained (CG) system, one bead can represent a group of atoms or even several molecules. Similar to molecular dynamics simulations, the time evolution of particles is governed by

Newton's equations of motion as eqn (1),

$$\frac{dr_i}{dt} = v_i, \quad m_i\frac{dv_i}{dt} = f_i \tag{1}$$

where $r_i$, $v_i$, $m_i$, and $f_i$ are the position, velocity, mass and force of the $i$ bead, respectively. The DPD method uses the reduced unit, with the mass of bead set to 1. The force $f_i$ acting on bead $i$ can be described *via* conservative force $F_{ij}^{C}$ representing the excluded volume effect, the dissipative force $F_{ij}^{D}$ representing vicious drag, the random force $F_{ij}^{R}$ representing the stochastic impulse, the spring force $F_{ij}^{S}$, and the electrostatic force $F_{ij}^{E}$ by eqn (2).[59,60]

$$f_i = \sum_{j\neq i} F_{ij}^{C} + F_{ij}^{D} + F_{ij}^{R} + F_{ij}^{S} + F_{ij}^{E}, \tag{2}$$

The interaction between the beads is determined by cutoff radius reduced unit $r_c$, which is set to 1. The length unit $r_c$ can be converted to the real length unit by equation $r_c = (\rho \times N_m \times V_w)^{1/3}$. Specifically, the first three forces are determined by the positions and velocities of beads $i$ and $j$, as given by eqn (3)–(5),

$$F_{ij}^{C} = \begin{cases} a_{ij}(1 - r_{ij})\hat{r}_{ij} & (r_{ij} < 1) \\ 0 & (r_{ij} \geq 1) \end{cases}, \tag{3}$$

$$F_{ij}^{D} = -\gamma\omega^{D}(r_{ij})(\hat{r}_{ij}v_{ij})\hat{r}_{ij}, \tag{4}$$

$$F_{ij}^{R} = \sigma\omega^{R}(r_{ij})\theta_{ij}\hat{r}_{ij}, \tag{5}$$

where $r_{ij} = r_j - r_i$, $r_{ij} = |r_{ij}|$, $\hat{r}_{ij} = r_{ij}/|r_{ij}|$, and $v_{ij} = v_j - v_i$, $a_{ij}$ is the maximum repulsion parameter between particle $i$ and $j$, $\gamma$ is the dissipation strength, $\sigma$ denotes the noise amplitude; $\theta_{ij}$ is a random number with zero mean and unit variance; $\omega^{D}(r_{ij})$ and $\omega^{R}(r_{ij})$ are $r$-dependent weight functions. According to the fluctuation–dissipation theorem, Español and Warren[61] showed a relationship between the two weight functions, as eqn (6) and (7),

$$\omega^{D}(r_{ij}) = [\omega^{R}(r_{ij})]^2 = \begin{cases} (1 - r_{ij})^2 & (r_{ij} < 1) \\ 0 & (r_{ij} \geq 1) \end{cases}, \tag{6}$$

$$\sigma^2 = 2\gamma k_B T, \tag{7}$$

where $T$ is the absolute temperature and $k_B$ is the Boltzmann's constant. In our simulation systems, the value of $\gamma$ is set to 4.5 and $\sigma$ is set to 3. The spring force between two adjacent beads of a certain molecule is expressed as

$$F_{ij}^{S} = \sum_{j} Cr_{ij}, \tag{8}$$

where $C$ is the dimensionless spring constant between beads $i$ and $j$, set to 4, according to the study by Groot and Warren,[54] which is sufficient to maintain a slightly smaller distance for bonded beads than for non-bonded beads.

The electrostatic force $F_{ij}^{E}$ is calculated by a modified Ewald sum method according to González–Melchor *et al.*,[62]

$$F_{ij}^{E} = \frac{\Gamma q_i q_j}{4\pi r_{ij}^2}[1 - \exp(-2\beta r_{ij})(1 + 2\beta r_{ij}(1 + \beta r_{ij}))]\hat{r}_{ij}, \tag{9}$$

where $\Gamma = e^2/(k_B T \varepsilon_0 \varepsilon_r r_c)$; $e$ is the electron charge; $\varepsilon_0$ and $\varepsilon_r$ are the dielectric constants of vacuum and water at room temperature, respectively; and $q$ denotes the particle charge; $\beta = r_c/\lambda$, where $\lambda$ is the decay length of the charge.

## Models and simulation parameters

The studied system is composed of a zwitterionic polymer, nanopore and water. In this work, the diameter and the length of the pore system is set as 30 and 42 $r_c$, respectively, which fits the definition of a nanopore. The CG models of the zwitterionic polymer and nanopore are shown in Fig. 1. The CG model of PCBMA contains three types of beads, B, N and C, which represent the backbone chain, the amino group and the carboxyl group, respectively (Fig. 1a). The zwitterionic polymers are grafted onto the nanopore *via* the fixed head beads (the fixed head bead is the B bead on the one end of PCBMA chain). The beads of the nanopore are denoted as P and the wall density of the nanopore is the same as that of the system with $\rho = 3$.[63,64]

Calculating the bead–bead repulsion parameter or DPD interaction parameter $a_{ij}$ is the most important step in DPD simulations. The repulsion parameters were obtained according to the following equations,[54,65]

$$\chi_{ij} = \frac{(\delta_i - \delta_j)^2 V}{RT} \tag{10}$$

$$a_{ij} = a_{ii} + 3.27\chi_{ij} \tag{11}$$

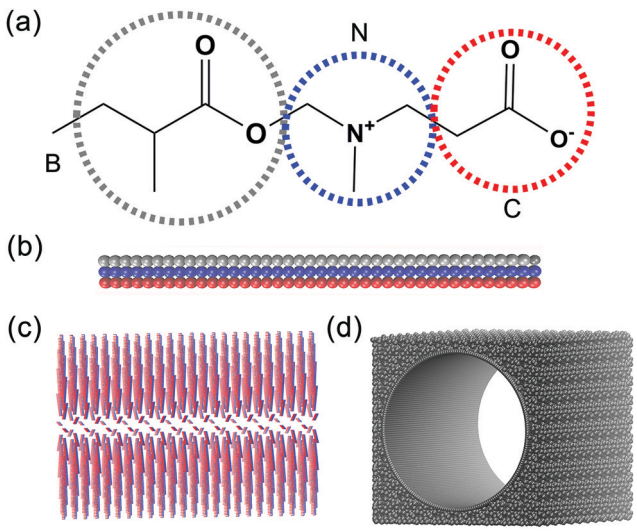


Fig. 1 The molecular structure and coarse-grained models of the PCBMA monomer (a), polymer chain (b); polymer brush (c) and nanopore (d).

 

Table 1 Repulsive parameters $a_{ij}$ between different beads at 298 K

| | B | N | C | W | P | $A^+$ | $A^-$ |
|---|---|---|---|---|---|---|---|
| B | 25.00 | | | | | | |
| N | 72.50 | 25.00 | | | | | |
| C | 27.00 | 89.42 | 25.00 | | | | |
| W | 78.64 | 57.78 | 51.81 | 25.00 | | | |
| P | 100.00 | 100.00 | 100.00 | 100.00 | 25.00 | | |
| $A^+$ | 78.64 | 57.78 | 51.81 | 25.00 | 100.00 | 25.00 | 25.00 |
| $A^-$ | 78.64 | 57.78 | 51.81 | 25.00 | 100.00 | 25.00 | 25.00 |

Note: $W$ is the water bead; $A^+$ and $A^-$, containing one positive and negative unit charge, are counter ion beads, which are used to keep the system electrically neutral depending on the net charge of the simulation system.

$$a_{ii} = k_B T \frac{k^{-1} N_m^{-1}}{2\alpha\rho} \quad (12)$$

In eqn (10), $\chi_{ij}$ is the Flory–Huggins parameter that represents the interaction parameters between beads $i$ and $j$, $V$ is the reference molar volume, $R$ is the ideal gas constant, $\delta_i$ and $\delta_j$ are the solubility parameters for beads $i$ and $j$, respectively, and $T$ is the temperature of the system. In eqn (11), $a_{ii}$ represents the repulsion parameter between beads of the same kind. In eqn (12), $\alpha$ is a constant with a value of $0.101 \pm 0.001$ and $N_m$ is the number of water molecules represented by one DPD water bead. $k^{-1}$ is dimensionless compressibility, and its value is about 15.98 at room temperature. $\rho_{DPD}$ is the number density of the system, which is chosen as $\rho = 3$; $k_BT$ represents the energy unit in DPD simulations as the unit temperature $k_BT$ =1. Therefore, the repulsion parameter between the same bead $a_{ii}$ is 25.00.

Table 1 shows the repulsion parameters $a_{ij}$ between different beads at 298 K. In the experiment, the nanopore in the polystyrene (PS) membrane is hydrophobic.[66] According to previous works,[67,68] the repulsive parameter between P and other beads is set as 100.

Moreover, the pH-responsive behaviours of zwitterion-modified nanopore in aqueous buffers are explored under neutral and highly acidic conditions. Under highly acidic conditions, PCBMA is fully protonated and charged. Hence, the counterions $A^+$ and $A^-$ are added to preserve the charge neutrality of the simulation systems. The repulsive parameters $a_{ij}$ of the counterions are the same as that of water. In order to explore the salt concentration-responsiveness properties, NaCl is chosen, the molar concentrations of salt ions were calculated[69] by $c^{real} = (N_{Na^+Cl^-}/V^*)/(r_c^3 N_A)$, where $N_{Na^+Cl^-}$ is the number of salt ion pairs and $N_A$ is the Avogadro number. The repulsive parameters of $Na^+$ or $Cl^-$ beads are the same as those of counter ion $A^+$ or $A^-$ beads.

### Simulation

In this work, DPD simulations are conducted using the DL_MESO 2.5 package.[70] The system is a cubic box with a box length of $35 \times 35 \times 42\ r_c$, where $r_c$ is the basic length unit in DPD simulations. The pore size is set to $\Phi = 30\ r_c$ with a length of $42\ r_c$. To ensure that the final states of the systems reach equilibrium, a step size of $\Delta t = 0.05\ \tau$ was employed, where $\tau = 1$ is the reduced DPD time unit, the simulation steps are at least $4 \times 10^5$, the periodic boundary conditions were applied in all three directions. The Ewald sum approach was used in long-range electrostatic interactions, electrostatic cutoff $r_C^{ele} = 3$, real-space convergence parameter $\alpha = 0.975$, and reciprocal space ($k$-vector) range $k_{max} = (5, 5, 5)$.

## Results and discussion

PCBMA has side chains composed of cationic quaternary ammonium and anionic carboxylate functional groups, the latter can be easily converted into other functional groups. Due to its ultralow fouling, functionalizability, biomimetic, biocompatible and noncytotoxic characters, PCBMA has been widely studied as a functional zwitterionic polymer. In this work, PCBMA has been chosen as functional brushes for grafting onto the nanopores to reveal the mechanisms of antifouling and stimuli-responsiveness properties. The model is shown in Fig. 1. The switching effect of zwitterionic modified nanopores can be modulated by two major factors, pH value and salt concentration. In addition, the polymer grafting density and chain length also have impacts at different pH and salt concentration conditions.

### pH-Controlled pore opening/closure

As shown in Fig. 1, the PCBMA polymer is charge neutral under neutral conditions. Whereas it is positively charged under acidic conditions due to the protonation of the carboxylic acid group. This intrinsic property of surface charge responsive to pH allows the conformation changes of PCBMA polymers, which further tunes surface properties with selective permeability. In this work, aiming to explore the pH-responsiveness of the PCBMA-modified nanopores, the performances under neutral and highly acidic conditions were discussed and compared. Additionally, the grafting density in this work is defined as the number of grafting chains per membrane area, and the chain length ($N$) means the polymerization degree of PCBMA. All units in this work are DPD simulation reduced units.

### Effect of grafting density

The effect of polymer grafting density on nanopores grafted PCBMA brushes as a smart switch is investigated with respect to the polymer chain length (the number of monomer unit) of 40. As shown in Fig. 2a, one can see that, under both neutral and acidic conditions, the nanopores maintain the open state at the lower polymer grafting density (0.169); however, from the lateral view of the nanopore, it clearly shows that zwitterionic polymers cannot cover the surface of the entire nanopore at lower grafting density under neutral conditions. As the grafting density increases to 0.192, the nanopore still remains open under neutral conditions. While under acidic conditions, the pore is partially open. As the grafting density further increases to 0.212, the state of the nanopore is distinct apparently: under neutral conditions, the pore size slightly reduces and still remains

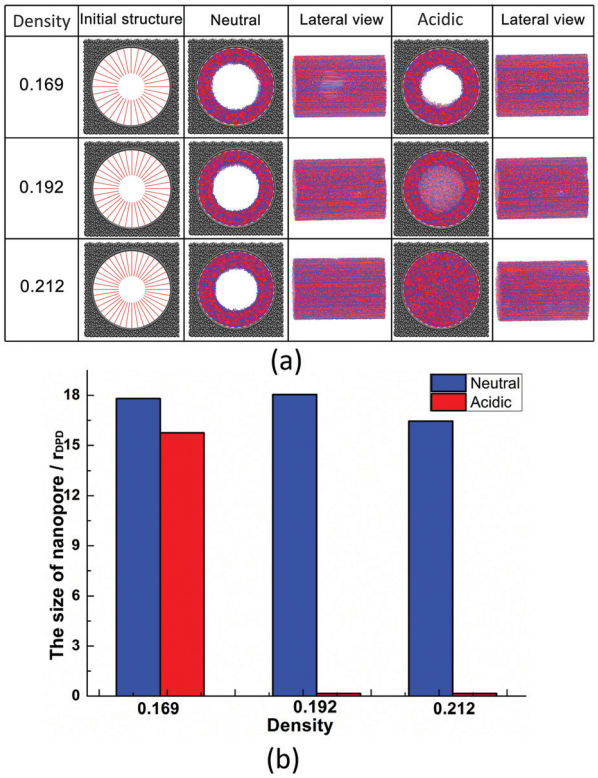


Fig. 2 (a) Morphologies of nanopores with different grafting densities under neutral and acidic conditions (blue, N beads; red, C beads; grey, nanopore beads and water beads are not shown, the same as below.), (b) the pore sizes of nanopores under neutral and acidic conditions.

open; while the pore closes completely under acidic conditions. To discover the change of the nanopore sizes clearly, Poreblazer 3.0.2 package[71] was adopted to quantitatively calculate the pore size. As observed in Fig. 2b, at the lower grafting density (0.169), the nanopore sizes decrease from 17.8 to 15.7 under neutral and acidic conditions. Differently, for systems with grafting densities of 0.196 and 0.212, the nanopore sizes are 18.0 and 16.5 under neutral conditions; while the nanopore sizes become zero under acidic conditions, which is consistent with the above simulation results.

The main reason for these performances is that under the neutral conditions, the zwitterionic polymer is electroneutral and the PCBMA chains tend to collapse or contract by inter and/or intrachain associations, giving rise to the nanopore-opening; as the pH transforms to the highly acidic, PCBMA is fully protonated and carries a positive charge; thus, the electrostatic repulsion increases, accompanying the interaction of inter and/or intrachain forces, eventually resulting in the extension of the PCBMA chains and the pore-closure. The potential energies of systems under different conditions also prove the results. The potential energy under neutral conditions is 9.69, while that under acidic conditions is 8.66. Moreover, to display the switching-off process clearly, the trajectory snapshots of conformation changes for the system of length 40 and grafting density 0.212 under highly acidic conditions are shown in Fig. 3. The more direct animation of the switching process can be observed from the video S1 in the ESI.†

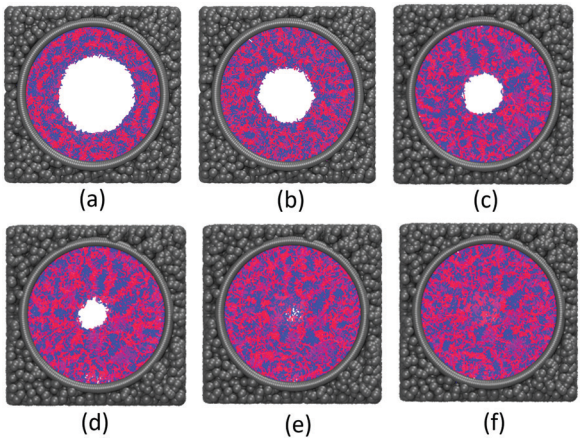


Fig. 3 The trajectory snapshots of conformation changes for the system of length 40 and grafting density 0.212 under highly acidic conditions, (a)step 0; (b) step 50 000; (c) step 100 000 (d) step 150 000; (e) step 200 000; and (f) step 250 000.

The simulation results are consistent with that of the previous work by Huo *et al.*[72] They explored different deprotonation degrees of PCBMA and found that with the decrease of pH, the deprotonation degree decreases, and the PCBMA segments extend. This also proves the reliability of our simulation result.

In addition, PCBMA as a typical polyzwitterion has strong hydration capabilities. The tightly bound, structured water layer around the zwitterionic pendant groups is induced electrostatically, which plays an important role in fouling-resistance. Therefore, proper grafting density is important to obtain an antifouling water layer. Experimental results by Xiang *et al.*[73] indicated that at the grafting densities larger than 20%, the nanopore exhibits antifouling properties. Furthermore, Wu *et al.*[74] also proposed that modified membranes with high grafting density possess better antifouling characteristics. All these agree with our simulation results. Since nanopore exhibits improved antifouling properties when the grafting density of zwitterionic polymer is higher than 20%, in the following sections, the grafting density of zwitterionic polymer brushes is set to 0.212.

### Effect of the chain length

At a constant grafting density of 0.212, the effect of PCBMA chain length (polymerization degree) on the nanopore switching is investigated. The simulation results are shown in Fig. 4a. Obviously, when the polymerization degree of PCBMA is 35, the nanopores remain open under both neutral and acidic conditions. As chain length increases by 5, there are different states of nanopores, in which the pores remain open and completely close under neutral and acidic conditions, respectively. As the chain length increases up to 45, the nanopores are both ''closed'' under neutral or highly acidic conditions. Thus, the nanopore switching effect cannot be achieved for short or long chain lengths. Gratifyingly, the smart pH-responsiveness switching can be achieved at the intermediate length of 40.

 

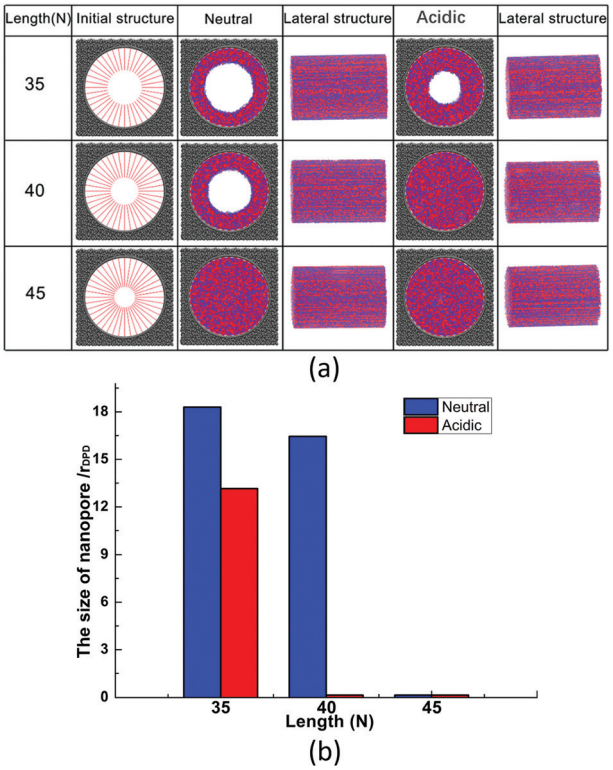


Fig. 4 (a) Morphologies of PCBMA with different grafted lengths under neutral and acidic conditions; (b) the pore sizes of nanopores under neutral and acidic conditions.

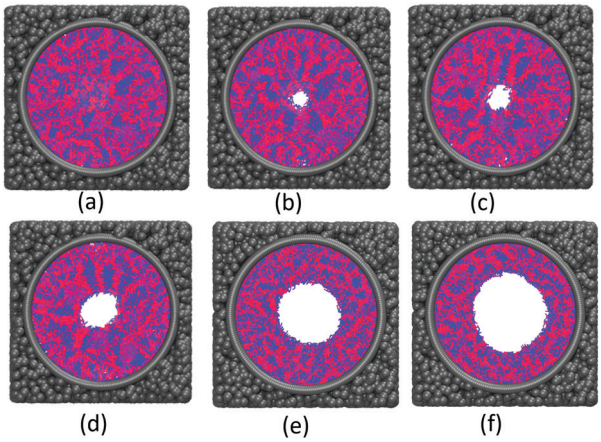


Fig. 5 The trajectory snapshots of conformation changes for the system of length 40 and grafting density 0.212 from highly acidic conditions to the neutral condition, (a) step 0; (b) step 50 000; (c) step 100 000 (d) step 150 000; (e) step 200 000; (f) step 250 000.

In addition, the pore sizes were calculated quantitatively. As depicted in Fig. 4b, at a length of 35, the nanopore under neutral conditions is 18.3, while under acidic conditions it is 13.2. The differences result from that under acidic conditions, zwitterion particles become charged, which leads to electrostatic repulsion between them; thus, the chains stretch. As the chain lengths increase under the neutral conditions, the nanopore sizes decrease from 18.3 to 16.5, and then to zero. While under the influence of protonation, under acidic conditions, the pore size becomes zero at a chain length of 40 and remains closed at a length of 45.

To verify the pH-responsive properties of the nanopore, taking the system of grafting density 0.212 as an example, the morphological changes of the nanopore have been observed from acidic conditions to the neutral conditions. The conformation changes are shown in Fig. 5 and the more detailed information can be observed from the video S1 in the ESI.† The size of the final nanopore is 16.3 which changes slightly compared with that (16.5) before switching-off. The result further confirmed that the zwitterionic polymer PCBMA modified nanopores achieve a reversible smart on–off character, which is consistent with previous experimental results.[43,46]

The results indicate that, considering the factor of pH, to achieve a smart switching effect and satisfactory antifouling performance, it is better to choose a grafting density of 0.212 and a PCBMA chain length of 40. Moreover, the properties of pH-responsiveness and antifouling of porous membranes are favourable in some industrial applications, such as oil exploitation, industrial wastewater treatment, and drug delivery *in vivo*. Our simulation results might provide some instructions for functional material exploration in these applications.

## Salt concentration-controlled pore open/closure

Due to the presence of cationic quaternary ammonium and anionic carboxylate functional groups, the salt concentration may affect the electrostatic interaction of PCBMA, further affecting the brush performance in nanopores. Consequently, in this section, the effect of salt concentration on the switching of the nanopore was studied. As well as influences of grafting density and chain length were discussed.

***Effect of the grafting density.*** The effect of grafting density on the nanopore switching was studied at a salt concentration of 2.0 M and chain length 35. Simulation results shown in Fig. 6 indicate that, at a lower graft density 0.169, the nanopore remains open which is similar to the result under pH-responsive conditions. While, when the grafting density of zwitterionic polymer brushes range over 0.192 ∼ 0.212, the nanopores show the close state, which differs from the states under pH-responsive conditions. The results further illustrate that compared with the pH effect, salt concentration has a more dramatic effect on the switching of nanopore.

***Effect of the chain length.*** The effect of the PCBMA chain length on the nanopore switching is also discussed, with the grafting density of zwitterionic polymer of 0.192 and salt concentration of 2.0 M. The simulation results are shown in Fig. 7. It is found that when the PCBMA chain length is 30, the nanopore is open; while as the chain lengths increase to 35–40, the nanopore is closed. These results are really different from those under pH-responsive conditions, under which the closed switch appears in middle length 40 rather than 45, namely, the switching effect of nanopore modified by PCBMA brushes become more sensitive to the salt concentration compared with the solution pH.

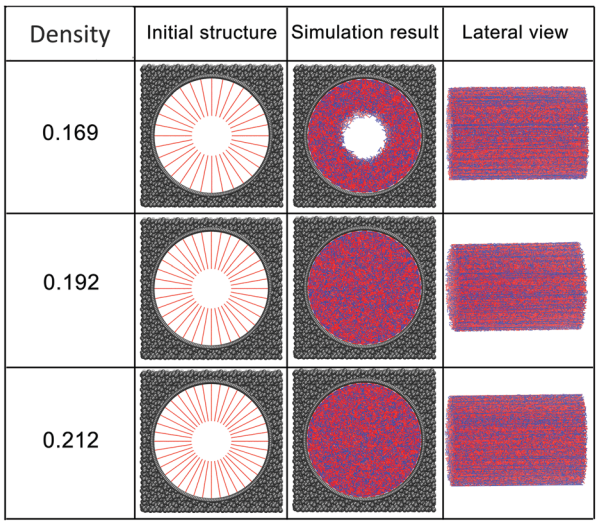


Fig. 6 Morphologies of nanopores with different grafting densities at high salt concentrations.

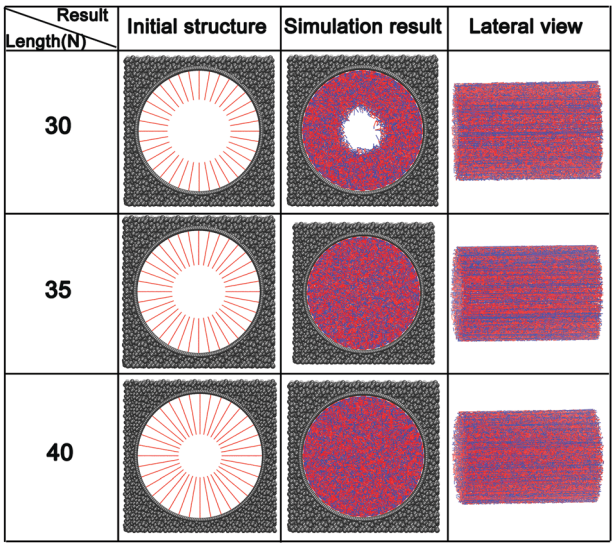


Fig. 7 Morphologies of nanopores with different chain lengths at high salt concentrations.

The experimental result of Wu *et al.* demonstrated that the flow control and antifouling performances were positively correlated with the grafting density and chain length.[74] The simulation result in this work can give guidance for choosing certain grafting density and chain length to realize both antifouling and dual-responsiveness performance of the nanopore in the flow control field.

***Effect of salt concentration.*** Based on the above results, in this section, grafting density 0.192 was chosen to explore the effect of salt concentration on nanopore switching. Additionally, to more clearly characterize the influence of the salt concentration on the nanopore size, the chain length 30 was adopted. According to results shown in Fig. 8a, it can be seen that nanopores remain open, and pore sizes are almost

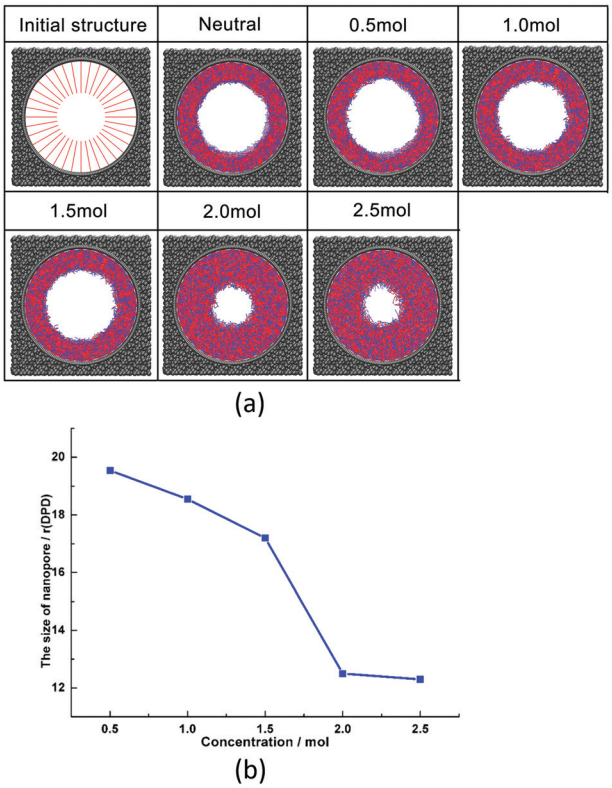


Fig. 8 (a) Morphologies of nanopores under different salt concentrations; (b) pore sizes of nanopores under different salt concentrations.

constant at lower salt concentrations ranging from 0.5 to 1.5 M. When the salt concentration was increased to 2.0 M, the pore size decreases rapidly, but further increasing it to 2.5 M, the pore size slightly shrinks. Quantitative pore size calculation at different concentrations is shown in Fig. 8b. The pore sizes slightly decrease from 19.7, 18.6 to 17.2 as the salt concentration increases from 0.5 to 1.5 M. When the salt concentration increases to 2.0 M, the pore size of the nanopore reduced directly to 12.4; whereas the salt concentration increased to 2.5 M, the pore size remains almost unchanged, which indicates that nanopore size reaches a threshold value under higher salt solution conditions. Therefore, in order to form a closed nanopore, a high salt concentration is required. This is consistent with the experimental result of Xiang *et al.*[73]

This phenomenon is related to the special structure of zwitterionic polymer PCBMA. When it is in a salt solution, the positive or negative ions of salt solution assemble at the cationic quaternary ammonium or anionic carboxylate groups due to the electrostatic interactions. It can weaken the self-association between cationic and anionic groups of PCBMA. Therefore, the zwitterionic polymer PCBMA shrinks at low salt concentrations due to the self-association between quaternary ammonium or carboxylate groups; as the salt concentrations increase, the self-association between cationic and anionic groups weakens and causes the polymer chain to gradually swell, which leads to nanopore shrinkage. Until the salt concentration continues to increase, the size of the nanopore changes slightly.

 

Liao *et al.*[75] and Chen *et al.*[47] explored the effect of ionic strength with NaCl salt on the underwater oleophobicity of a zwitterionic system. They found that the addition of salt weakened the self-association between zwitterion molecules, which led to the enhancement of hydration, which indicated the improvement of antifouling properties. Actually, these agree with the result in this work, and our work gives a clear morphology of PCBMA at different salt concentrations, which further contributes to understanding the mechanism of PCBMA conformation transition at different salt concentrations at the molecular level and provides guidance for experimental synthesis.

## Conclusions

In summary, DPD simulations were performed to study the switching effect of zwitterionic polymer-brush-modified nanopores at the mesoscale level. Due to the intrinsic structure, nanopores modified by PCBMA brushes display pH and salt concentration dual-responsiveness. In addition, the grafting density and chain length of the zwitterionic polymer PCBMA have a significant effect on the switching of nanopores under different pH and salt concentration conditions.

The simulation results show that nanopores modified by PCBMA brushes show obvious pH-responsiveness. In detail, the grafting density has a greater effect on the nanopore switching under different pH conditions. At lower grafting densities, the inner surface of the nanopore cannot be fully covered under any pH condition, so its antifouling performance is not ideal. When the grafting density is 0.212, zwitterionic polymers can cover the entire nanopore, and it can form completely closed nanopores under acidic conditions. Therefore, a relatively high grafting density should be chosen to prepare smart nanopores. Moreover, the effect of different chain lengths on the nanopore switching was also investigated. When the chain length is too short, closed nanopores cannot be formed under any pH condition, but when the chain length is too long, the nanopore is always closed. Therefore, the switching effect of nanopores can only be achieved with a relatively medium chain length of 40.

On the other hand, nanopores modified by PCBMA display salt-concentration-responsiveness which can affect the switching. It is found that the grafting density and chain length of zwitterionic polymers also play a certain role in nanopore switching at different salt concentrations. Compared with results under pH-responsive conditions, the switching effect of the nanopore can be achieved at a relatively lower grafting density of 0.192 and a relatively shorter chain length of 35, which means that the nanopore switching is more sensitive to the salt concentration. Finally, the influence of salt concentration on the nanopore size is explored. It is found that the pore size decreases at low salt concentrations (0.5 to 1.5 M), but when the salt concentration is increased to 2.0 M, the pore size decreases obviously. If the salt concentration continues to increase, the pore size shrinks little, and an even higher salt concentration is required to form a closed nanopore. By comparing the effects of salt concentration and pH on the switching of nanopores, it was found that the salt concentration has a relatively stronger effect on the switching.

These results can provide the molecular mechanism and theoretical guidance for designing smart nanopores modified by a zwitterionic polymer, and the smart nanopore will play an important role in anti-fouling and biomedical applications. Deeply, we hope that this work can supply some guidelines for the development of zwitterion-modified nanopores in smart nanoflow control devices.

## Author contributions

Zhaohong Miao performed the experiments, data analysis, investigation, paper writing and original manuscript revision; Zheng Chen performed data analysis, investigation and original manuscript revision; Li Wang performed the experiments, data analysis and original manuscript revision; Lizhi Zhang performed the manuscript revision; Jian Zhou designed the concept, supervised the experiments and manuscript revision. All authors contributed to the general discussion.

## Conflicts of interest

There are no conflicts of interest to declare.

## Acknowledgements

This work was supported by the National Natural Science Foundation of China (No. 51936005 and 21776093) and the GuangDong Basic and Applied Basic Research Foundation (2022A1515010876). We also thanks to the GPU hours provided by the SCUTGrid at the South China University of Technology.

## Notes and references

1 I. Banerjee, R. C. Pangule and R. S. Kane, *Adv. Mater.*, 2011, **23**, 690–718.
2 J. N. Shen, H. M. Ruan, L. G. Wu and C. J. Gao, *Chem. Eng. J.*, 2011, **168**, 1272–1278.
3 M. P. Schultz, J. A. Bendick, E. R. Holm and W. M. Hertel, *Biofouling*, 2011, **27**, 87–98.
4 T. S. Wong, S. H. Kang, S. K. Y. Tang, E. J. Smythe, B. D. Hatton, A. Grinthal and J. Aizenberg, *Nature*, 2011, **477**, 443–447.
5 J. Yin and B. L. Deng, *J. Membr. Sci.*, 2015, **479**, 256–275.
6 I. Amara, W. Miled, R. B. Slama and N. Ladhari, *Environ. Toxicol. Pharmacol.*, 2018, **57**, 115–130.
7 W. Yang, H. S. Sundaram, J. R. Ella, N. He and S. Jiang, *Acta Biomater.*, 2016, **40**, 92–99.
8 E. H. Leduc and S. J. Holt, *J. Cell Biol.*, 1965, **26**, 137–155.
9 A. L. Lewis, Z. L. Cumming, H. H. Goreish, L. C. Kirkwood, L. A. Tolhurst and P. W. Stratford, *Biomaterials*, 2001, **22**, 99–111.

10 H. W. Ma, J. H. Hyun, P. Stiller and A. Chilkoti, *Adv. Mater.*, 2004, **16**, 338–341.
11 J. Zheng, L. Y. Li, H. K. Tsao, Y. J. Sheng, S. F. Chen and S. Y. Jiang, *Biophys. J.*, 2005, **89**, 158–166.
12 G. Mantovani, F. Lecolley, L. Tao, D. M. Haddleton, J. Clerx, J. J. L. M. Cornelissen and K. Velonia, *J. Am. Chem. Soc.*, 2005, **127**, 2966–2973.
13 R. F. A. Zwaal and A. J. Schroit, *Blood*, 1997, **89**, 1121–1132.
14 S. F. Long, S. Clarke, M. C. Davies, A. L. Lewis, G. W. Hanlon and A. W. Lloyd, *Biomaterials*, 2003, **24**, 4115–4121.
15 B. Mrabet, M. N. Nguyen, A. Majbri, S. Mahouche, M. Turmine, A. Bakhrouf and M. M. Chehimi, *Surf. Sci.*, 2009, **603**, 2422–2429.
16 C. Yoshikawa, A. Goto, Y. Tsujii, T. Fukuda, T. Kimura, K. Yamamoto and A. Kishida, *Macromolecules*, 2006, **39**, 2284–2290.
17 E. Ostuni, R. G. Chapman, R. E. Holmlin, S. Takayama and G. M. Whitesides, *Langmuir*, 2001, **17**, 5605–5620.
18 M. C. Shen, L. Martinson, M. S. Wagner, D. G. Castner, B. D. Ratner and T. A. Horbett, *J. Biomater. Sci., Polym. Ed.*, 2002, **13**, 367–390.
19 Y. Kadoma, *Egypt. J. Text. Polym. Sci. Technol.*, 1978, **35**, 423–427.
20 K. Ishihara, T. Ueda and N. Nakabayashi, *Polym. J.*, 1990, **22**, 355–360.
21 Y.-N. Chou, A. Venault, Y.-H. Wang, A. Chinnathambi, A. Higuchi and Y. Chang, *J. Mater. Chem. B*, 2018, **6**, 4909–4919.
22 A. Venault, Y. W. Bai, G. V. Dizon, H. Y. E. Chou, H. C. Chiang, C. T. Lo, J. Zheng, P. Aimar and Y. Chang, *J. Mater. Chem. B*, 2019, **7**, 7184–7194.
23 P. Liu, Q. Chen, L. Li, S. Lin and J. Shen, *J. Mater. Chem. B*, 2014, **2**, 7222–7231.
24 Q. Shao and S. Y. Jiang, *Adv. Mater.*, 2015, **27**, 15–26.
25 X. Peng, H. L. Liu, Q. Yin, J. C. Wu, P. Z. Chen, G. Z. Zhang, G. M. Liu, C. Z. Wu and Y. Xie, *Nat. Commun.*, 2016, **7**, 1–8.
26 T. Chen, F. Wu, Z. Chen, J. Huo, Y. Zhao, L. Zhang and J. Zhou, *J. Colloid Interface Sci.*, 2021, **587**, 173–182.
27 V. B. Damodaran and N. S. Murthy, *Biomater. Res.*, 2016, **20**, 18.
28 S. Y. Fam, C. F. Chee, C. Y. Yong, K. L. Ho, A. R. Mariatulqabtiah and W. S. Tan, *Nanomaterials*, 2020, **10**, 787.
29 M.-C. Sin, S.-H. Chen and Y. Chang, *Polym. J.*, 2014, **46**, 436–443.
30 A. Q. Wang, W. X. Fang, J. Y. Zhang, S. J. Gao, Y. Z. Zhu and J. Jin, *Small*, 2020, **16**, 1903925.
31 W. Guo, H. Xia, L. Cao, F. Xia, S. Wang, G. Zhang, Y. Song, Y. Wang, L. Jiang and D. Zhu, *Adv. Funct. Mater.*, 2010, **20**, 3561–3567.
32 Z. Chen, J. Huo, L. Hao and J. Zhou, *Curr. Opin. Chem. Eng.*, 2019, **23**, 21–33.
33 Q. Chen, J. Bai, J. Li, K. Huang, X. Li, B. Zhou and W. Cai, *Chem. Eng. J.*, 2014, **252**, 89–94.
34 J. Peng, N. Zhao, S. Lin, W. Wang, M. J. Zhang, Y. Y. Su, R. Xie, X. J. Ju, Z. Liu and L. Y. Chu, *Chem. Eng. J.*, 2021, **407**, 127138.
35 L. Chu, R. Xie and X. Ju, *Chin. J. Chem. Eng.*, 2011, **19**, 891–903.
36 Z. Liu, W. Wang, R. Xie, X. J. Ju and L. Y. Chu, *Chem. Soc. Rev.*, 2016, **45**, 460–474.
37 C. G. Palivan, R. Goers, A. Najer, X. Zhang, A. Car and W. Meier, *Chem. Soc. Rev.*, 2016, **45**, 377–411.
38 S. Q. Zhang, T. Sun and J. H. Wang, *Microchim. Acta*, 2015, **182**, 1387–1393.
39 Y. Liu, D. Zhang, B. Ren, X. Gong, L. Xu, Z. Q. Feng, Y. Chang, Y. He and J. Zheng, *J. Mater. Chem. B*, 2020, **8**, 3814–3828.
40 Y. Wang, J. Wu, D. Zhang, F. Chen, P. Fan, M. Zhong, S. Xiao, Y. Chang, X. Gong, J. Yang and J. Zheng, *J. Mater. Chem. B*, 2019, **7**, 5762–5774.
41 C. Lavigueur, J. G. García, L. Hendriks, R. Hoogenboom, J. J. L. M. Cornelissen and R. J. M. Nolte, *Polym. Chem.*, 2011, **2**, 333–340.
42 X. Hou, W. Guo and L. Jiang, *Chem. Soc. Rev.*, 2011, **40**, 2385–2401.
43 Z. Siwy, D. Dobrev, R. Neumann, C. Trautmann and K. Voss, *Appl. Phys. A: Mater. Sci. Process.*, 2003, **76**, 781–785.
44 H. Alem, A.-S. Duwez, P. Lussis, P. Lipnik, A. M. Jonas and S. Demoustier-Champagne, *J. Membr. Sci.*, 2008, **308**, 75–86.
45 Z. Y. Jiang, L. Y. Chu, X. M. Wu, Z. Wang, X. B. Jiang, X. J. Ju, X. H. Ruan and G. H. He, *Rev. Chem. Eng.*, 2020, **36**, 67–105.
46 B. Yameen, M. Ali, R. Neumann, W. Ensinger, W. Knoll and O. Azzaroni, *J. Am. Chem. Soc.*, 2009, **131**, 2070–2071.
47 Z. Chen, M. R. Liao, L. Z. Zhang and J. Zhou, *AIChE J.*, 2021, **67**, e17103.
48 J. Huo, H. Jiang, Z. Chen and J. Zhou, *Chem. Eng. Sci.*, 2018, **191**, 490–499.
49 M. Belkin, S. H. Chao, G. Giannetti and A. Aksimentiev, *J. Comput. Electron.*, 2014, **13**, 826–838.
50 B. X. Xu, B. L. Wang, T. Park, Y. Qiao, Q. L. Zhou and X. Chen, *J. Chem. Phys.*, 2012, **136**, 184701.
51 E. Madai, M. Valisko and D. Boda, *J. Mol. Liq.*, 2019, **283**, 391–398.
52 S. Zeng, X. Quan, H. Zhu, D. Sun, Z. Miao, L. Zhang and J. Zhou, *Langmuir*, 2021, **37**, 1225–1234.
53 P. Espanol and P. B. Warren, *J. Chem. Phys.*, 2017, **146**, 150901.
54 R. D. Groot and P. B. Warren, *J. Chem. Phys.*, 1997, **107**, 4423–4435.
55 Z. Chen, L. Wang and J. Zhou, *CIESC J.*, 2019, **70**, 271–279.
56 A. Z. Niu, D. J. Liaw, H. C. Sang and C. Wu, *Macromolecules*, 2000, **33**, 3492–3494.
57 J. Ladd, Z. Zhang, S. Chen, J. C. Hower and S. Jiang, *Biomacromolecules*, 2008, **9**, 1357–1361.
58 P. J. Hoogerbrugge and J. M. V. A. Koelman, *EPL*, 1992, **19**, 155–160.
59 R. D. Groot and K. L. Rabone, *Biophys. J.*, 2001, **81**, 725–736.
60 R. D. Groot, *J. Chem. Phys.*, 2003, **119**, 10454.
61 P. Espanol and P. Warren, *EPL*, 1995, **30**, 191–196.
62 M. Gonzalez-Melchor, E. Mayoral, M. E. Velazquez and J. Alejandre, *J. Chem. Phys.*, 2006, **125**, 224107.
63 Q. Q. Cao, C. C. Zuo, L. J. Li, Y. J. Li and Y. Yang, *Biomicrofluidics*, 2012, **6**, 034101.
64 Q. Q. Cao, C. C. Zuo, L. J. Li, Y. H. Zhang and G. Yan, *J. Polym. Sci., Part B: Polym. Phys.*, 2012, **50**, 805–811.

 

65 R. D. Groot and T. J. Madden, *J. Chem. Phys.*, 1998, **108**, 8713–8724.
66 I. Velzeboer, C. Kwadijk and A. A. Koelmans, *Environ. Sci. Technol.*, 2014, **48**, 4869–4876.
67 Z. Posel, Z. Limpouchová, K. Šindelka, M. Lísal and K. Procházka, *Macromolecules*, 2014, **47**, 2503–2514.
68 W. Li, W. Chu and Z. Jian, *Chem. Res. Chin. Univ.*, 2018, **39**, 85–94.
69 E. Meneses-Juarez, C. Marquez-Beltran, J. F. Rivas-Silva, U. Pal and M. Gonzalez-Melchor, *Soft Matter*, 2015, **11**, 5889–5897.
70 M. A. Seaton, R. L. Anderson, S. Metz and W. Smith, *Mol. Simul.*, 2013, **39**, 796–821.
71 L. Sarkisov and A. Harrison, *Mol. Simul.*, 2011, **37**, 1248–1257.
72 J. Huo, Z. Chen and J. Zhou, *Langmuir*, 2018, **35**, 1973–1983.
73 T. Xiang, C. D. Luo, R. Wang, Z. Y. Han, S. D. Sun and C. S. Zhao, *J. Membr. Sci.*, 2015, **476**, 234–242.
74 J. J. Wu, J. Zhou, J. Q. Rong, Y. Lu, H. Dong, H. Y. Yu and J. S. Gu, *Chin. J. Polym. Sci.*, 2018, **36**, 528–535.
75 M. Liao, G. Cheng and J. Zhou, *J. Phys. Chem. C*, 2017, **121**, 17390–17401.